Published in final edited form as:
*Cancer Res*. 2019 January 01; 79(1): 183–195. doi:10.1158/0008-5472.CAN-18-1397.

# miR-146a controls immune response in the melanoma microenvironment

**Justin Mastroianni**[1,2], **Natalie Stickel**[1], **Hana Andrlova**[1], **Kathrin Hanke**[1,2], **Wolfgang Melchinger**[1], **Sandra Duquesne**[1], **Dominik Schmidt**[1,2], **Martina Falk**[1], **Geoffroy Andrieux**[3], **Dietmar Pfeifer**[1], **Heide Dierbach**[1], **Annette Schmitt-Graeff**[4], **Frank Meiss**[5], **Melanie Boerries**[3], and **Robert Zeiser**[1,6]

[1]Department of Hematology, Oncology and Stem Cell Transplantation, Freiburg University Medical Center, Albert Ludwigs University (ALU) Freiburg, Freiburg, Germany

[2]Faculty of Biology, Albert-Ludwigs-University, Freiburg, Germany

[3]Institute of Molecular Medicine and Cell Research, IMMZ, ALU, Freiburg, Germany. German Cancer Consortium (DKTK), Freiburg, Germany. German Cancer Research Center, (DKFZ), Heidelberg, Germany

[4]Institute of Surgical Pathology, Freiburg University Medical Center, Albert-Ludwigs-University, Freiburg, Germany

[5]Department of Dermatology, Freiburg University Medical Center, Albert-Ludwigs-University, Freiburg, Germany

[6]CIBSS – Centre for Integrative Biological Signalling Studies, University of Freiburg

## Abstract

Micro-RNAs (miR) are small non-coding RNAs that regulate gene expression, post-transcription, and manipulate immune responses in different types of cancer. In this study, we identify miR-146a as a negative regulator of immune activation, comparable to immune checkpoint molecules. miR-146a levels were increased in melanoma microenvironmental tissue, and miR-146a-/- mice survived longer and developed less metastases in comparison to wild type melanoma-bearing mice. T cells isolated from miR-146a-/- mice revealed higher expression levels of the miR-146a target gene Stat1 and the Stat1-regulated cytokine Interferon-γ (IFN-γ). Neutralization of IFN-γ in miR-146a-/- mice decreased survival and increased melanoma metastasis patterns to those of wild-type mice. In vitro, IFN-γ reduced melanoma cell migration, cell cycle activity, and basal metabolic rate. Conversely, IFN-γ also increased PD-L1 levels on the melanoma cells, which may counterbalance some of the beneficial effects increasing immune escape in vivo. Combined treatment with a miR-146a antagomiR and anti-PD-1 resulted in improved survival over isotype-control or anti-PD-1 treatment alone. In summary, these data show that miR-146a plays a central role within the STAT1/IFN-γ axis in the melanoma microenvironment, affecting melanoma

**Corresponding Author:** Robert Zeiser, MD, Section for Tumor Immunology, Department of Hematology, Oncology and Stem Cell Transplantation, University of Freiburg, Hugstetter Str. 55, 79106 Freiburg, Germany, Tel.: 0761 270 34580, Fax.: 0761 270 73570, robert.zeiser@uniklinik-freiburg.de.

Conflict of Interest Statement: The authors have declared that no conflict of interest exists.


Europe PMC Funders Author Manuscripts

migration, proliferation, and mitochondrial fitness as well as PD-L1 levels. Additionally, combined inhibition of PD-1 and miR-146a could be a novel strategy to enhance anti-tumor immune response elicited by checkpoint therapy.

**Keywords**

miR-146a; immune checkpoint inhibitors; melanoma; microenvironment; Interferon-γ

## Introduction

The treatment of patients with metastatic melanoma with combined immune checkpoint inhibition leads to impressive response rates and improved overall survival compared to conventional chemotherapy (1). However, a maximum of 15% of patients respond to the anti-CLTA4 therapy, or 40% to anti-PD-1 therapy. Moreover, 30-50% of patients develop adverse-events related to the therapy, independent of disease response to therapy (1). Therefore additional combinations of immune checkpoint inhibitors and strategies that target molecules in the tumor microenvironment are an important area of investigation. For example, inhibition of immunosuppressive CD73 (2) or LAG3 (3) holds promise to improve the response rate to immune checkpoint inhibitors of patients with metastatic tumors including melanoma.

microRNAs (miRs) are highly conserved short 21–25 nucleotide non-coding RNAs that bind and post-transcriptionally regulate mRNA translation. miRNAs affect multiple target genes yielding a phenotype that could augment immune checkpoint inhibition. Therefore combination therapy, aimed at manipulati specific miRNAs in addition to immune checkpoint inhibition, is a potent prospect. One example, miR-21, plays a significant role in multiple cancer types and is an attractive target for Small Molecular Inhibitors of Specific miRNAs (SMIR). Different studies on compounds which inhibit this miRNA have shown anti-cancer activity in preclinical models (4,5). miR-34 is transcriptionally induced by p53 and is decreased in many types of cancer, leading to tumor genesis and increased PD-L1 on the tumor cell surface (6). miR-146a is a major regulator of multiple pro-inflammatory events (7) including effects on the TRAF6/TNF axis in T cells (8) and the JAK/STAT/MHC axis in antigen presenting cells (9). Therefore, it holds promise to play a central role in immune cells residing in the melanoma microenvironment. We found that miR-146a is a central negative regulator of the STAT1/IFN-γ axis in the melanoma microenvironment. As IFN-γ reduces melanoma migration, proliferation and mitochondrial fitness and because miR-146a blocks these beneficial anti-tumor effects; we tested targeting of this miR to enhance anti-tumor immunotherapy. Indeed, the combination of anti-PD1 blockade and miR-146a antagomiR synergistically improved the survival outcome *in vivo*, supporting the novel concept of a combined antagomiR / immune checkpoint inhibitor therapy.





Europe PMC Funders Author Manuscripts

## Materials and Methods

### Human tissue analysis

The study included formalin-fixed and paraffin-embedded (FFPE) tissue specimens of primary tumors from 22 patients that underwent surgery for the treatment of melanoma, 18 nevocellular nevi and 13 unremarkable healthy skin samples. We obtained written informed consent from all patients prior to analysis. The studies were conducted in accordance with the ethical guidelines of the Declaration of Helsinki and the studies were approved by an institutional review board, and by the local ethics committee (protocol no.: 569/15; Ethic committee, Albert-Ludwigs-University, Freiburg, Germany). Melanoma patients treated within a time period of 10 years (2002-2012) at the Dept. of Dermatology, University Hospital Freiburg, Germany, from whom a biopsy was available, were analyzed.

### TaqMan quantitative reverse transcription PCR (qRT-PCR) for miRNA expression in human skin

For analysis of miR-146a expression in human melanoma, nevocellular nevus and healthy skin samples, total RNA from FFPE tissue was isolated using the miRNeasy FFPE Kit (Qiagen) according to the manufacturer's instructions. MultiScribe Reverse Transcriptase was used for reverse transcription and miR-146a expression was examined with the TaqMan MicroRNA Assay Kit (Life technologies) and a LightCycler 480 (Roche). TaqMan primers for hsa miR 146a (assay ID 000468) were used to monitor miRNA expression. Gene expression was normalized to the reference gene snoRNA202 (assay ID 001232) and data were analyzed using the Pfaffl method.

### Mice

C57BL/6 wild type and *miR146a*$^{-/-}$ mice (C57BL/6 background) mice were obtained from the local animal facility of the University Medical Center Freiburg, Germany and bred under special pathogen-free conditions in the Mouse Experimental Unit of the animal facility. BRaf$^{CA}$, Pten$^{loxP}$, Tyr::CreERT2 mice were provided by Prof. Dr. Burkhard Becher from the University of Zurich. The genotype of gene-targeted mice was confirmed by polymerase chain reaction (PCR). Mice were used for *in vivo* experiments at between 6 and 12 weeks of age and 15-25 g of weight. All animal studies had been approved by the University institutional review board on the Use and Care of Laboratory Animals at the Albert-Ludwigs University Freiburg, Germany (Protocol approval numbers: G-13/116, G17-049, X13-07J, X15-10A).

### Mouse melanoma models

WT and *miR-146a*$^{-/-}$ mice were both injected with 1x10$^4$ B16.F10 luc$^+$ melanoma cells in the tail vein. Afterwards, their survival was monitored and bioluminescence images (BLI) were captured as described previously (10). In another experiment, the mice were sacrificed on day 20-24 and the tumors, lungs, lymph nodes, and metastases were resected for further examination. For the second melanoma model, 2x10$^6$ 4434 melanoma cells were injected intravenously (i.v.) in the tail vein and survival was monitored. Subcutaneous models for melanoma involved injecting 1x10$^5$ B16.F10 luc$^+$ melanoma cells into WT and *miR-146a*$^{-/-}$

mice. Tumor growth was monitored via BLI and palpation. The tumors and organs were then isolated from mice euthanized on day 20-24. A genetic melanoma mouse model was used to simulate a disease similar to which is found in patients ($BRaf^{CA}$, $Pten^{loxP}$, $Tyr::Cre^{ERT2}$) (11). The BRaf/Pten mice received 2μl of 4-HT (Hydroxytamoxifen, 5mM) on the shorn right flank, on Day 0, Day 2, and Day 4. Tumors were then monitored and size documented. When the tumor of the BRaf/Pten mice reached 15mm on a single axis, the mice were euthanized and the tumors, organs and metastases resected for further studies.

### *In vivo* antibody and oligonucleotide inhibitor treatment

WT and *miR-146a*$^{-/-}$ mice received 200μl intraperitoneal (i.p.) injections of Isotype control antibody (200μg/mouse /treatment) (Rat IgG1, κ; Biolegend, cat#400427) or IFN-γ blocking antibody (200μg/mouse/treatment) (R4.6A2, Biolegend, cat#505707) on day 0, 4, 8, and 12.

For translational *in vivo* experiments, WT mice injected with melanoma in the tail vein on day 0, received anti-PD-1 antibody, i.p. on days 1, 4 8, 16, and 22. Control mice were treated in parallel with an Armenian hamster isotype control purchased from BioXcell, (cat# BE0091). Oligonucleotides inhibiting miRNA-146a (ThermoFisher mirVana™ miRNA Inhibitor, Cat#: 4464088 ID: MH10722) or scramble controls (ThermoFisher mirVana™ miRNA Inhibitor, Negative Control #1, Cat#: 4464079) were administered via tail vein injections on days 5 and 9. *In vivo*-jetPEI® (Polyplus, cat# 201-50G), facilitated *in vivo* delivery of oligonucleotides across cell membranes, for 60μg of oligonucleotides injected in 200μl volume of 5% Glucose/*in vivo*-jet-PEI, per product protocol.

### LPS treatment

WT or *miR-146a*$^{-/-}$ mice were injected i.p. with 1 mg/kg LPS from Salmonella enterica (Sigma-Aldrich) in 100 μL PBS on days 0, 7 and 14. Mice were sacrificed and T cells analyzed for IFN-γ production using flow cytometry on day 22.

### Hematopoietic chimera generation

To generate chimeric mice that lacked miR-146a either in the complete hematopoietic compartment or T lymphocyte specific compartment we used a previously described method (12). Briefly, on day -14, Wild type (WT) (C57BL/6) recipients were transplanted with $5x10^6$ *miR-146a*$^{-/-}$ or WT bone marrow cells i.v. after TBI with 11Gy (2 x 5.5Gy). On day 0, mice received $1x10^4$ B16-Luc$^+$ tumor cells, as well as, $5x10^4$ *miR-146a*$^{-/-}$ or WT T cells i.v. Mice were then monitored for survival and for metastases via BLI.

### Bioluminescence imaging

For *in vivo* bioluminescence imaging (BLI), luciferin [D-Luciferin, potassium salt (S)-4,5-Dihydro-2-(6-hydroxy-2-benzothiazolyl)-4-thiazolecarboxylic acid potassium salt; Biosynth] was injected intraperitoneally (i.p.) at a concentration of 150 μg/g body weight (10). After 10 minutes, mice were imaged using an IVIS100 CCD imaging system (Xenogen) with an exposure time of 5 minutes. The signal from luciferase transgenic cells was quantified in photons per second per mouse. Acquisition, analysis and visualization of bioluminescence imaging were performed using Living Image Software. For the

bioluminescence imaging measurements the following parameters were kept constant for the WT and the *miR-146a*$^{-/-}$ groups: the amount and type of luciferin, the imaging exposure time of 5 minutes, and distance to camera determined by field of view of 12.5cm.

## Cell lines

B16.F10 murine melanoma cell line was provided by Prof. H. Pircher, Freiburg, Germany. Transducing the cells with a lentiviral vector containing firefly luciferase, a neomycin resistance gene, and green-fluorescent protein (GFP) produced a transgenic line of the B16.F10 luc$^{+}$. B16.F10 luc$^{+}$ were selected with 2mg/ml of the neomycin analog Geneticin (G-418 Sulfate). Melanoma cells were > 95% positive for GFP prior to i.v. injection (Suppl. Figure S1). BRAF-mutant 4434 mouse melanoma cell lines were established from C57BL/6 LSL-Braf$^{V600E}$; Tyr::CreERT2$^{+/o}$ mice (13) and were provided by Dr. Richard Marais, Manchester, UK. The B16 cell line was authenticated by Eurofins Medigenomix GmbH, Ebersberg, Germany, as previously described (10). All cells were cultured at 37°C in 5% $CO_2$.

## Western Blot

CD4$^{+}$ and CD8$^{+}$ T cells were isolated from secondary lymphoid organs of mice using MACS beads. T cells restimulated with PMA (500ng/ml) and Ionomycin (50ng/ml), or CD3/CD28 Dynabeads from ThermoFisher Scientific, were then lysed with RIPA (Santa Cruz Biotechnology, Inc.) lysis buffer containing Phosphatase Inhibitor Cocktail 2 (Sigma Aldrich). BCA protein assay (Pierce) ascertained protein concentrations of each lysate. Proteins were separated based on size in SDS-PAGE gradient gels (4-12%), then transferred to polyvinylidene fluoride (PVDF) membranes from Amersham Biosciences. Membranes were then blotted for proteins with specific antibodies. After the antibody incubation a chemiluminescent substrate for the peroxidase was applied to membranes, followed by imaging on the INTAS ECL Chemocam Imager. Quantification of Western blots was done using Lab1image software. The uncut gels of the western blots are shown in Suppl. Figure S2-S7.

## Antibodies

**Western Blot antibodies—**The following primary detection antibodies with respective concentrations: rabbit anti-mouse Stat1 (polyclonal) antibody, Cell Signaling Technology cat#9172, 1:1000; rabbit anti-mouse phospho-Stat1 (Y701) (clone: 58D6) antibody, Cell Signaling Technology cat#9167, 1:1000 rabbit anti-mouse Stat3 (clone: 79D7) antibody, Cell Signaling Technology cat#4904, 1:1000; rabbit anti-mouse phospho-Stat3 (Y705) (polyclonal) antibody, Cell Signaling Technology cat#9167, 1:1000; rabbit anti-mouse Stat5 (clone: D206Y) antibody, Cell Signaling Technology cat#94205, 1:1000; rabbit anti-mouse phospho-Stat5 (Y694) (clone: C11C5) antibody, Cell Signaling Technology cat#9359, 1:1000; rabbit anti-mouse β-actin (clone: 13E5) antibody, Cell Signaling Technology cat#4967, 1:2000; mouse anti-mouse GAPDH (Clone: GAPDH-71.1) HRP-linked antibody, 1:35000, Sigma-Aldrich, cat#G9295. After one-hour incubation with a primary antibody, a secondary antibody was used for non-HRP labeled antibodies: goat anti-rabbit IgG HRP-linked antibody, Cell Signaling Technology cat#7074, at dilutions of 1:2000-10000.

**Antibodies for flow cytometry—**Flow cytometry was used to determine protein levels on living cells. The following extra-cellular antibodies were used: CD3-APC (clone: 17A2), CD8-FITC (clone: 53-6.7), Rat IgG1, κ-PE isotype control (clone: eBRG1), from eBioscience; CD8a-APC (clone: 53-6.7), PD-1 (CD279)-PE_Cy7 (clone: 29F.1a12), PD-L1 (CD274)-APC (clone: 10F.9G2), CD4-Alexafluor647 (clone: GK1.5), Rat IgG2a, κ-FITC (clone: RTK2758), Rat IgG2b-Alexafluor 647(clone: RTK4530), Rat IgG2b, κ-APC (clone: RTK4530), κ-FITC (clone:RTK2758), from Biolegend. For intracellular protein staining we used anti-IFN-γ-Alexafluor 647 (clone: XMG1.2), anti-IFN-γ-PE (clone: XMG1.2) from eBioscience. Cell viability was monitored with either propidium iodide, from Sigma-Aldrich, Fixable Viability Dye -eFluor780, from eBioscience, or Aquablue Live/Dead Stain from ThermoFisher Scientific; depending on the experiment requirements. Data were acquired on a Fortessa (BD Biosciences) or a CyAn ADP (Beckman Coulter) and analyzed using FlowJo v10.

### *STAT1* gain-of-function in primary murine WT Tcells

*STAT1* gain-of-function (GOF) mutations have been previously documented in patients (14). A plasmid encoding the *STAT1* GOF mutation transgene (R321G) on a pMX-_Ires_GFP backbone was used to make retrovirus, packaged in phoenix cells. Pan T-cells isolated from WT mice (8-12 weeks) using Pan T Cell Isolation Kit II, Miltenyi (130-095-130) were infected with virus containing either the *STAT1* GOF either or the empty vector, as control. Prior to infection, T cells were activated with CD3/CD28 Dynabeads (ThermoFisher, 11456D) in the presence of IL-2 from Immunotools (R12340024), for 24 hours. before being submitted to three repeat spin infections (300xG, 90min, 32°C) were then performed on $3x10^6$ T cells/well in Retronectin from Clonetech, (T100B) coated 6-well plates. Viral infection efficiency was then measured via FACS as $GFP^+$ events. We have previously described the use of this STAT1 GOF mutation (15).

### miRNA expression analysis by Taqman qRT-PCR

Total RNA was isolated from tumor and surrounding microenvironmental tissues with the Qiagen miRNeasy RNA extraction micro kit (cat# 217084). miRNAs were then reverse transcribed into cDNA with specific probes using TaqMan™ MicroRNA Reverse Transcription Kit, from ThermoFisher Scientific. TaqMan primers for hsa-miR-146a (assay ID 000468) were used to monitor miRNA expression. Gene expression was normalized to reference genes snoRNA202 (assay ID 001232), or snU6 (assay ID 001973) and the relative expression was compared to the untreated or negative control group (Pfaffl method).

### xCELLigence proliferation assay

Proliferation studies were performed on the xCELLigence® RTCA DP instrument. Serum was removed from cell culture media 24 hours prior to the start of the experiment. E-plate® from xCELLigence® was seeded with $1,5x10^5$ B16 cells per well with variable levels of IFN-γ (0 ng/ml, 10n/ml, 100ng/ml, 1μg/ml). Cell index as a measure of electric impedance was measured for 96 hours.

### Wound healing migration assay

Ibidi® 2-well inserts were seeded with $3x10^5$ B16 cells per well in serum-containing media and incubated for 6 hours to allow adherence. Media was then replaced with serum-free DMEM or serum-free DMEM containing IFN-γ (100ng/ml) and cells were incubated at 37°C in 5% $CO_2$ incubator. The silicone insert was removed 24 hours after IFN-γ induction in serum-free media thereby initiating gap for migration. IFN-γ treated B16 migration was compared to non-treated control as a function of gap closure.

### Microarray analysis

B16.F10 cells were stimulated with IFN-γ (100ng/ml) in 6-well plates. After 40 hours of stimulation, total RNA was isolated from cells using a Qiagen miRNeasy Micro Kit. RNA quality was assessed using an Agilent 2100 Bioanalyzer (Agilent Technologies). Microarray was performed using Affymetrix Clariom S Assay for mouse genes.

Tissues and tumors (200mg maximum mass) were isolated from $BRaf^{CA}$, $Pten^{loxP}$, $Tyr::Cre^{ERT2}$ were isolated for total RNA isolation using the same RNA isolation kit. RNA quality was assessed as previously mentioned. Microarray was performed using the Affymatrix GeneChip™ miRNA 4.0 Array and FlashTag™ Biotin HSR RNA Labeling Kit (ThermoFisher Scientific).

ArrayExpress accession numbers:

**E-MTAB-6372** : Expression data from total RNA from B16 murine melanoma cells stimulated with interferon-γ versus untreated controls

**E-MTAB-6373**: Transcription profiling by array of miRNA in mouse models of melanoma comparing niches of tumor tissue to adjacent normal tissue

### Differential analysis

A Linear model based approach (limma R package) (16) was used to identify the differentially regulated RNA between interferon-γ stimulated (n=5) and unstimulated (n=4) B16.F10 cells. Similarly, we compared miRNA in mice tumors (n=3) vs. healthy skin tissues (n=3) from $BRaf^{CA}$, $Pten^{loxP}$, $Tyr::Cre^{ERT2}$ mice. Regulated RNA and miRNA with Benjamini Hochberg adjusted P value < .05 were set as significant.

### Statistical analysis

Statistical analyses were performed with GraphPad Prism Version 4/5 or 7 software. Data are reported as mean ± SEM or SD. Kaplan-Meier survival curves were analyzed by log-rank tests (Mantel-Cox test). Group comparisons were performed with a 2-tailed unpaired Student *t* test. *P* values < .05 were considered to be statistically significant. In fold change data analysis, 2- tailed one sample *t* test was performed on one experimental group with $H_0$=1, and again P values < .05 were considered significant.

All other methods are detailed in the Suppl. methods section.

## Results

### *miR-146a*$^{-/-}$ mice experience reduced melanoma growth and survive better which is connected to increased IFN-γ production by *miR-146a*$^{-/-}$ T cells

To determine whether miR-146a was expressed in the melanoma microenvironment we isolated melanoma tissue from *BRaf*$^{CA}$ *Pten*$^{loxP}$ *Tyr::Cre*$^{ERT2}$ mice that develop local melanoma upon local tamoxifen exposure and analyzed the expression of multiple micro RNAs. We found higher miR-146a expression in the metastatic melanoma tissue compared to control tissue isolated from the same site of a tumor free mouse without the Cre recombinase (Figure 1A). To assess the influence of miR-146a on metastatic melanoma progression we then injected melanoma cells intravenously into WT or *miR-146a*$^{-/-}$ mice. Survival of melanoma-bearing *miR-146a*$^{-/-}$ mice was improved compared to WT mice, a result observed with two different melanoma cell lines (4434 or B16 murine melanoma cells) (Figure 1B, C). In agreement with the improved survival, the luciferase signal derived from expanding B16 luc$^{+}$ melanoma cells (Figure 1D) and the number of GFP$^{+}$ melanoma cells isolated from the lungs of melanoma bearing mice was lower in *miR-146a*$^{-/-}$ mice compared to WT mice (Figure 1E, F). Melanoma cells were more than 95% positive for GFP prior to i.v. injection (Suppl. Figure S1). These findings indicate that a lack of miR-146a has a beneficial effect on control of melanoma growth *in vivo*.

To clarify the mechanism responsible for the improved survival of the melanoma bearing *miR-146a*$^{-/-}$ mice, we analyzed the cytokine production of T cells isolated from WT versus *miR-146a*$^{-/-}$ mice treated with LPS. We observed a significant increase in IFN-γ producing T cells in *miR-146a*$^{-/-}$ mice compared to WT mice (Figure 1G, H).

In order to verify if the increase of IFN-γ producing T cells was functionally relevant for the improved survival of *miR-146a*$^{-/-}$ mice compared to WT mice, we treated melanoma bearing *miR-146a*$^{-/-}$ mice with a neutralizing anti-IFN-γ antibody or an unspecific IgG antibody. Treatment of melanoma bearing *miR-146a*$^{-/-}$ mice with a neutralizing anti-IFN-γ antibody led to a loss of survival benefit, comparable to that of WT mice (Figure 1I). Treatment of melanoma bearing WT mice with a neutralizing anti-IFN-γ antibody caused no significant difference in survival, compared to WT mice treated with the unspecific IgG (Figure 1J), emphasizing the dependence of *miR-146a*$^{-/-}$ mice on IFN-γ for prolonged survival.

### *In vivo* IFN-γ-neutralization antagonizes the control of melanoma growth in *miR-146*$^{-/-}$ mice

To understand the effect of IFN-γ neutralization on melanoma growth we analyzed the expansion of luciferase-transgenic melanoma cells *in vivo.* The melanoma-derived photon flux was steady until after day 14, when the tumors started to expand. We observed that the melanoma-derived BLI signal was higher in the *miR-146a*$^{-/-}$ mice treated with a neutralizing anti-IFN-γ antibody compared to *miR-146a*$^{-/-}$ mice treated with an unspecific control antibody (Figure 2A, B).

The observed hyperactivity in the Stat1/IFN-γ axis in T cells led to the hypothesis that they contribute to improved survival. Thus, to validate the source of the survival mediating IFN-γ, we created a hematopoietic chimera model in which we reconstituted hematopoietic cells and T cells with combinations of WT cells or cells lacking *miR-146a*. We observed

improved survival in all groups receiving T cells which lack miR-146a, while deficiency of *miR-146a* in hematopoietic cells, excluding T cells, was not sufficient for the protective effect (Figure 2C). We explain this by the observation that most IFN-γ production is derived from the adoptively transferred T cells while newly generated T cells from the BM play a minor role. In agreement with that hypothesis we found only a minor trend towards improved survival when the BM lacked miR-146a while survival was significantly improved when the adoptively transferred T cells lacked miR-146a. It is possible that also other immune cells play a role in the miR-146a mediated local immune suppression in the melanoma microenvironment.

When comparing T cells isolated from the lungs of tumor-bearing versus naive mice we observed that expression of miR-146a increased in T cells isolated from the melanoma bearing mice (Figure 2D). This novel finding supports the concept that miR-146a plays a major role in T cells that interact with melanoma cells in the tumor microenvironment. These findings indicate that the partial protection from melanoma-related death in melanoma bearing *miR-146a*$^{-/-}$ mice is due to IFN-γ produced by T cells.

## Increased IFN-γ levels are due to Stat1 activation in *miR-146*$^{-/-}$ T cells

As Stat1 phosphorylation and dimerization is known to activate IFN-γ production, we next analyzed the levels of Stat1 and pStat1. Stat1 total protein increased in *miR-146a*$^{-/-}$ T cells isolated from spleens and lymph nodes of melanoma bearing mice compared to WT mice (Figure 3A, B). In agreement with this observation Stat1 has been previously shown to be a target of miR-146a (17). Furthermore, Stat3 and Stat5 protein did not increase in *miR-146a*$^{-/-}$ T cells and are not predicted targets of miR-146a (Figure 3C, D). Also, phosphorylated-Stat1 increased in *miR-146a*$^{-/-}$ T cells isolated from spleens and lymph nodes of melanoma bearing mice compared to wildtype controls (Figure 3E, F). To validate the proposed STAT1/IFN-γ axis in our system we infected wild type T cells with virus containing a STAT1 gain-of-function (GOF) mutation (R321G). We observed that T cells containing this STAT1 GOF mutation produced more IFN-γ compared to T cells containing empty vector control (Figure 3G, H). These findings indicate that *miR-146*$^{-/-}$ T cells exhibit increased activity of the STAT1/IFN-γ axis.

## IFN-γ affects cell cycle progression, migration and metabolism of melanoma cells *in vitro*

In well-controlled *in vitro* systems, we investigated the effects of IFN-γ on melanoma cells. We observed that multiple genes promoting cell cycle progression were downregulated in B16 melanoma cells when exposed to IFN-γ compared to the control group (Figure 4A). In agreement with the reduction of cell cycle related genes seen on the transcriptional level, IFN-γ significantly reduced the proliferation of B16 melanoma cells compared to controls when analyzed with the xCELLigence® system (Figure 4B). IFN-γ exposure reduced the expression of multiple genes involved in epithelial to mesenchymal transition (EMT) in melanoma cells (Figure 4C). Functionally, melanoma cells migrated less in scratch assays in the presence of IFN-γ compared to the control group (Figure 4D, E). Moreover, multiple Tricarboxylic Acid Cycle-related genes were down regulated when melanoma cells were exposed to IFN-γ compared to the control group (Suppl. Figure S8A). Consistent with changes in melanoma cell metabolism upon IFN-γ exposure, we observed a lower basal

oxygen consumption rate (OCR) in melanoma cells exposed to IFN-γ (Suppl. Figure S8B). We also analyzed production of reactive oxygen species (ROS) in melanoma cells in the presence versus absence of IFN-γ. We observed that ROS production increased in the melanoma cells upon IFN-γ exposure (Suppl. Figure S8C, D).

These data indicate that IFN-γ affects proliferation, cell cycle regulation and metabolism in melanoma cells.

## IFN-γ leads to upregulation of immunosuppressive PD-L1 on melanoma cells

Exposure of melanoma cells to IFN-γ increased the expression of multiple genes involved in immune responses, in particular PD-L1 (CD274) (Figure 5A). Increased PD-L1 expression was also found on the protein level when melanoma cells were exposed to IFN-γ *in vitro* (Figure 5B). To understand if these in vitro findings are relevant for the in vivo situation we next analyzed PD-L1 levels on melanoma cells isolated from WT or miR-146a mice. PD-L1 expression was higher on melanoma cells isolated from the lungs of miR-146a$^{-/-}$ mice compared to the melanoma cells isolated from the lungs of WT mice (Figure 5C).

These findings suggested that the IFN-γ induced upregulation of PD-L1 could promote immune escape of melanoma cells *in vivo*, which at the same time may render melanoma sensitive to immune checkpoint inhibition. We therefore tested survival of melanoma bearing wild type mice when treated with anti-PD-1 antibody or isotype control antibody. When anti-PD-1 antibody treatment was combined with miR-146a inhibiting nucleotides, the survival was significantly prolonged compared to mice receiving anti-PD-1 antibody and a non-specific scrambled nucleotide control in two different melanoma models (Figure 5D, E). Extended treatment periods of the miR-146a antagomir plus anti-PD-1 antibody also caused improved survival of the antagomir/anti-PD-1 group (Suppl. Figure S9A, B). In agreement with improved survival the mice treated with the combination of anti-PD-1 antibody and miR-146a antagomiR exhibited lower tumor burden as determined by bioluminescence imaging of mice bearing luciferase-transgenic B16 melanoma cells compared to the other groups (Figure 5F). Consistent with an effect of the miR-146a antagomir we found an increase of PD-L1 expression upon exposure of the melanoma cells to IFN-γ and the miR-146a antagomir compared to the exposure of the melanoma cells to IFN-γ alone (Suppl. Figure S10A, B). We also found that the tStat1 and pStat1 / GAPDH ratios increased in IFN-γ and/or IFN-γ + miR146a antagomir treated melanoma cells compared to untreated cells (Suppl. Figure S10C, D). For tStat1 and pStat1 no further increase by the IFN-γ + miR146a antagomir treatment over the IFN-γ treatment alone was observed (Suppl. Figure S10C, D). IFN-γ is known to be a strong activator of Stat1 and possibly the miR146a antagomir could not further enhance Stat1 transcription and activation as the maximum was already reached.

## miR-146a is increased in human melanoma tissue

To understand if miR-146a is found in human melanoma, we performed qPCR of melanoma tissue, healthy skin and nevi tissue. We found a significantly higher miR-146a expression in melanoma tissue specimen compared to nevi and compared to healthy skin (Figure 6A).

Also the melanoma tumor grade (TNM) correlated with the level of miR-146a as T4 tumors exhibited higher miR-146a levels than T1 or T2 tumors (Figure 6B).

Based on our findings we propose the following mechanism: miR-146a is produced in the tumor microenvironment to prevent activation of the STAT1/IFN-γ axis (Suppl. Figure S11). This can be antagonized by treatment with miR-146a antagomir leading to increased IFN-γ production. IFN-γ affects melanoma cell proliferation, migration and spare respiratory capacity but also increased PD-L1 levels. Increased PD-L1 expression upon miR-146a inhibition provides a scientific rationale to combine this treatment with immune checkpoint inhibition.

## Discussion

The treatment with immune checkpoint inhibitors and BRAF/MEK inhibitors has dramatically improved the clinical outcome of patients with metastatic melanoma. However there is still considerable fraction of patients that progress despite those therapies due to primary or secondary resistance. Resistance to therapy can be mediated by many cells in the tumor microenvironment such as regulatory T cells (18), myeloid derived suppressor cells that produce arginase (reviewed in (19)), cancer associated fibroblasts (20) and others. Overcoming these immunosuppressive mechanisms in order to make immune checkpoint inhibition more effective is a major goal and subject of intensive preclinical and clinical research. In preclinical studies activation of Toll-like Receptor 9 in combination with immune checkpoint inhibition have led to promising response rates (21). Strategies that have reached clinical trial level include inhibition of immunosuppressive LAG3 (3) and adenosine receptor inhibition (22).

Here we analyzed the role of miR-146a in the melanoma microenvironment based on its increased expression at tumor sites of $BRaf^{CA}$ $Pten^{loxP}$ Tyr::CreERT2 mice and found that mice lacking miR-146a achieved a better melanoma control. Since increased immune activation in *miR-146a*$^{-/-}$ mice (7,17) and patients (23,24) with a polymorphism that leads to less functional, mature miR-146a have been reported we then deciphered which miR-146a target genes, pathways and cytokines may be relevant in the context of the melanoma microenvironment.

We found that the miR-146a target Stat1 was upregulated in T cells of tumor bearing mice, which may be in response to more Stat1 protein originating from the STAT1/IFN-γ axis, in addition to miR-146a interfering directly with Stat1 translation through the RISC pathway. In agreement with a higher activity of this signaling pathway we also found increased levels of pStat1, which is downstream of the IFN-γ receptor and plays a critical role in Th1 immune responses (17). IFN-γ was particularly interesting in the context of the melanoma microenvironment because previous reports had shown that it can block neovascularization of tumor tissue which reduced melanoma growth (25) and IFN-γ production plays a key role for the antitumor effect of IL-12 (26).

We then observed that the increase in IFN-γ was T cell-derived and that its neutralization antagonized the beneficial effects of miR-146a deficiency.

Mechanistically, IFN-γ reduced cell-migration, cell cycle activity, and basal oxygen consumption rate in melanoma cells. These effects in concert with the previously reported anti-tumor effects of IFN-γ (25,26) may be responsible for the beneficial effects of miR-146a deficiency, which unleashes the STAT1/ IFN-γ axis. Consistent with our results, other studies have shown that IFN-γ inhibits growth and downregulates multiple genes involved in G-protein signaling, phospholipase C activation and cell cycling in three different human melanoma cell lines (27).

However, IFN-γ also increased PD-L1 levels on the melanoma cells, which may counterbalance some of the beneficial effects, inducing immune escape *in vivo*. To test this hypothesis we compared the combination therapy of miR-146a antagomiR with anti-PD-1 versus anti-PD-1 treatment alone, and isotype with scrambled oligonucleotide controls. Our observation that melanoma bearing mice exhibited an improved survival when treated with the miR-146a antagomiR / anti-PD1 combination compared to anti-PD-1 treatment alone supports the concept that miR-146a mediated suppression of the STAT1/IFN-γ axis diminishes some of the anti-melanoma immune activity. This phenomenon can be reversed with antagomiR combined with anti-PD1 antibody treatment.

In summary, we show that miR-146a plays a central role for the STAT1/IFN-γ axis in the melanoma microenvironment, thereby affecting melanoma migration, proliferation and metabolism, but also increasing PD-L1 levels. The combination of anti-PD1 blockade and miR-146a antagomiR enhanced melanoma control in two models, indicating its value as a novel strategy to enhance anti-tumor immune response to checkpoint-therapy.

## Supplementary Material

Refer to Web version on PubMed Central for supplementary material.

## Acknowledgements

$BRaf^{CA}$, $Pten^{loxP}$, Tyr::CreERT2 mice were provided by Prof. Dr. Burkhard Becher from the University of Zurich, Zurich, Switzerland.

PD-1 blocking antibody kindly provided by Dr. Bruce Blazar, from Department of Pediactrics, division of Blood and Marrow Transplantation, University of Minnesota, Minneapolis, Mn, USA.

B16.F10 murine melanoma cell line was provided by Prof. H. Pircher, Albert-Ludwigs Universität Freiburg, Germany.

BRAF-mutant 4434 mouse melanoma cell lines were established from C57BL/6 LSL-$Braf^{V600E}$; Tyr::$CreERT2^{+/0}$ mice (13) and were provided by Dr. Richard Marais, Cancer Research UK Manchester Institute, Manchester, UK.

Financial Support: This study was supported by the Deutsche Forschungsgemeinschaft, Germany, SFB 850 (C6 and Z2 to R.Z., Z1 to M.B.), and ERC Consolidator grant (ERC-2015-COG 681012 GvHDCure to R.Z.), the Excellence Strategy of the German Federal and State Governments (CIBSS - EXC 2189).

## References

1. Larkin J, Chiarion-Sileni V, Gonzalez R, Grob JJ, Cowey CL, Lao CD, Schadendorf D, Dummer R, Smylie M, Rutkowski P, Ferrucci PF, et al. Combined Nivolumab and Ipilimumab or Monotherapy in Untreated Melanoma. N Eng J Med. 2015; 373:23–34.

2. Allard B, Pommey S, Smyth MJ, Stagg J. Targeting CD73 enhances the antitumor activity of anti-PD-1 and anti-CTLA-4 mAbs. Clin Cancer Res. 2013; 19:5626–35. [PubMed: 23983257]
3. Ascierto PA, Melero I, Bhatia S, et al. Initial Efficacy of Anti-Lymphocyte Activation Gene-3 (anti-LAG-3; BMS-986016) in Combination With Nivolumab in Patients With Melanoma Previously Treated With Anti-PD-1/PD-L1 Therapy. J Clin Oncol. 2017; 15:9520–20.
4. Shi Z, Zhang J, Qian X, Han L, Zhang K, Chen L, Liu J, Ren Y, Yang M, Zhang A, Pu P, et al. AC1MMYR2, an inhibitor of dicer-mediated biogenesis of Oncomir miR-21, reverses epithelial-mesenchymal transition and suppresses tumor growth and progression. Cancer Res. 2013; 73:5519–31. [PubMed: 23811941]
5. Yan LX, Wu QN, Zhang Y, Li YY, Liao DZ, Hou JH, Fu J, Zeng MS, Yun JP, Wu QL, Zeng YX, et al. Knockdown of miR-21 in human breast cancer cell lines inhibits proliferation, in vitro migration and in vivo tumor growth. Breast Cancer Res. 2011; 13:R2. [PubMed: 21219636]
6. Craig VJ, Cogliatti SB, Imig J, Renner C, Neuenschwander S, Rehrauer H, Schlapbach R, Dirnhofer S, Tzankov A, Müller A. Myc-mediated repression of microRNA-34a promotes high-grade transformation of B-cell lymphoma by dysregulation of FoxP1. Blood. 2011; 117:6227–36. [PubMed: 21460242]
7. Boldin MP, Taganov KD, Rao DS, Yang L, Zhao JL, Kalwani M, et al. miR-146a is a significant brake on autoimmunity, myeloproliferation, and cancer in mice. J Exp Med. 2011; 208:1189–201. [PubMed: 21555486]
8. Stickel N, Prinz G, Pfeifer D, Hasselblatt P, Schmitt-Graeff A, Follo M, Thimme R, Finke J, Duyster J, Salzer U, Zeiser R. MiR-146a regulates the TRAF6/TNF-axis in donor T cells during GvHD. Blood. 2014; 124:2586–95. [PubMed: 25205119]
9. Stickel N, Hanke K, Marschner D, Prinz G, Köhler M, Melchinger W, Pfeifer D, Schmitt-Graeff A, Brummer T, Heine A, Brossart P, et al. MicroRNA-146a reduces MHC-II expression via targeting JAK/STAT-signaling in dendritic cells after stem cell transplantation. Leukemia. 2017; 31:2732–41. [PubMed: 28484267]
10. Andrlová H, Mastroianni J, Madl J, Kern JS, Melchinger W, Dierbach H, Follo M, Technau-Hafsi K, Has C, Mittapalli VR, Idzko M, et al. Biglycan expression in the melanoma microenvironment promotes invasiveness via increased tissue stiffness inducing integrin-β1 expression. Oncotarget. 2017; 8:42901–16. [PubMed: 28476030]
11. Dankort D, Curley DP, Cartlidge RA, Nelson B, Karnezis AN, Damsky WE Jr, You MJ, DePinho RA, McMahon M, Bosenberg M. Braf(V600E) cooperates with Pten loss to induce metastatic melanoma. Nat Genet. 2009; 41:544–52. [PubMed: 19282848]
12. Klämbt V, Wohlfeil SA, Schwab L, Hülsdünker J, Ayata K, Apostolova P, Schmitt-Graeff A, Dierbach H, Prinz G, Follo K, Prinz M, et al. A novel function for P2Y2 in myeloid recipient-derived cells during GvHD. J Immunol. 2015; 195:5795–804. [PubMed: 26538394]
13. Dhomen N, Reis-Filho JS, da Rocha Dias S, Hayward R, Savage K, Delmas V, Larue L, Pritchard C, Marais R. Oncogenic Braf induces melanocyte senescence and melanoma in mice. Cancer Cell. 2009; 15:294–303. [PubMed: 19345328]
14. Romberg N, Morbach H, Lawrence MG, Kim S, Kang I, Holland SM, Milner JD, Meffre E. Gain-of-function STAT1 mutations are associated with PD-L1 overexpression and a defect in B-cell survival. J Allergy Clin Immunol. 2013; 131:1691–3. [PubMed: 23403048]
15. Prestipino A, Emhardt A, Aumann K, O´Sullivan D, Gorantla SP, Duquesne S, Melchinger W, Braun L, Vuckovic S, Boerries M, Busch H, et al. Oncogenic JAK2V617F causes PD-L1 expression mediating immune-escape in myeloproliferative neoplasms. Sci Transl Med. 2018; 10(429):eaam7729. [PubMed: 29467301]
16. Ritchie ME, Phipson B, Wu D, Hu Y, Law CW, Shi W, Smyth GK. limma powers differential expression analyses for RNA-sequencing and microarray studies. Nucleic Acids Res. 2015; 43:e47. [PubMed: 25605792]
17. Lu LF, Boldin MP, Chaudhry A, Lin LL, Taganov KD, Hanada T, Yoshimura A, Baltimore D, Rudensky AY. Function of miR-146a in controlling Treg cell-mediated regulation of Th1 responses. Cell. 2010; 142:914–29. [PubMed: 20850013]
18. Dürr C, Pfeifer D, Claus R, Schmitt-Graeff A, Gerlach UV, Graeser R, Krüger S, Gerbitz A, Negrin RS, Finke J, Zeiser R. CXCL12 mediates immunosuppression in the lymphoma microenvironment

after allogeneic transplantation of hematopoietic cells. Cancer Res. 2010; 70:10170–81. [PubMed: 21159639]

19. Zeiser R, Blazar BR. Acute Graft-versus-host disease - Biologic process, prevention, and therapy. N Eng J Med. 2017; 377:2167–79.
20. Liu C, Liu L, Chen X, et al. LSD1 Stimulates Cancer-Associated Fibroblasts to Drive Notch3-Dependent Self-Renewal of Liver Cancer Stem-like Cells. Cancer Res. 2018; 78:938–49. [PubMed: 29259010]
21. Sagiv-Barfi I, Czerwinski DK, Levy S, Alam IS, Mayer AT, Gambhir SS, Levy R. Eradication of spontaneous malignancy by local immunotherapy. Science translational medicine. 2018; 10:426.
22. Young A, Ngiow SF, Barkauskas DS, et al. Co-inhibition of CD73 and A2AR Adenosine Signaling Improves Anti-tumor Immune Responses. Cancer Cell. 2016; 30:391–403. [PubMed: 27622332]
23. Bogunia-Kubik K, Wysoczańska B, Piątek D, Iwaszko M, Ciechomska M, Świerkot J. Significance of Polymorphism and Expression of miR-146a and NFkB1 Genetic Variants in Patients with Rheumatoid Arthritis. Arch Immunol Ther Exp. 2017; 64:131–36.
24. Jiménez-Morales S, Gamboa-Becerra R, Baca V, Del Río-Navarro BE, López-Ley DY, Velázquez-Cruz R, et al. MiR-146a polymorphism is associated with asthma but not with systemic lupus erythematosus and juvenile rheumatoid arthritis in Mexican patients. Tissue Antigens. 2012; 80:317–21. [PubMed: 22823586]
25. Qin Z, Blankenstein T. CD4+ T cell--mediated tumor rejection involves inhibition of angiogenesis that is dependent on IFN gamma receptor expression by nonhematopoietic cells. Immunity. 2000; 12:677–86. [PubMed: 10894167]
26. Nastala CL, Edington HD, McKinney TG, et al. Recombinant IL-12 administration induces tumor regression in association with IFN-g production. J Immunol. 1994; 153:1697–706. [PubMed: 7913943]
27. Gollob JA, Sciambi CJ, Huang Z, Dressman HK. Gene Expression Changes and Signaling Events Associated with the Direct Antimelanoma Effect of IFN-gamma. Cancer Res. 2005; 65:8869–77. [PubMed: 16204058]



Europe PMC Funders Author Manuscripts

Europe PMC Funders Author Manuscripts

## Statement of significance

Findings identify a micro-RNA based mechanism by which melanoma cells escape the immune system, providing a new therapeutic strategy to improve the current management of melanoma patients.

Europe PMC Funders Author Manuscripts

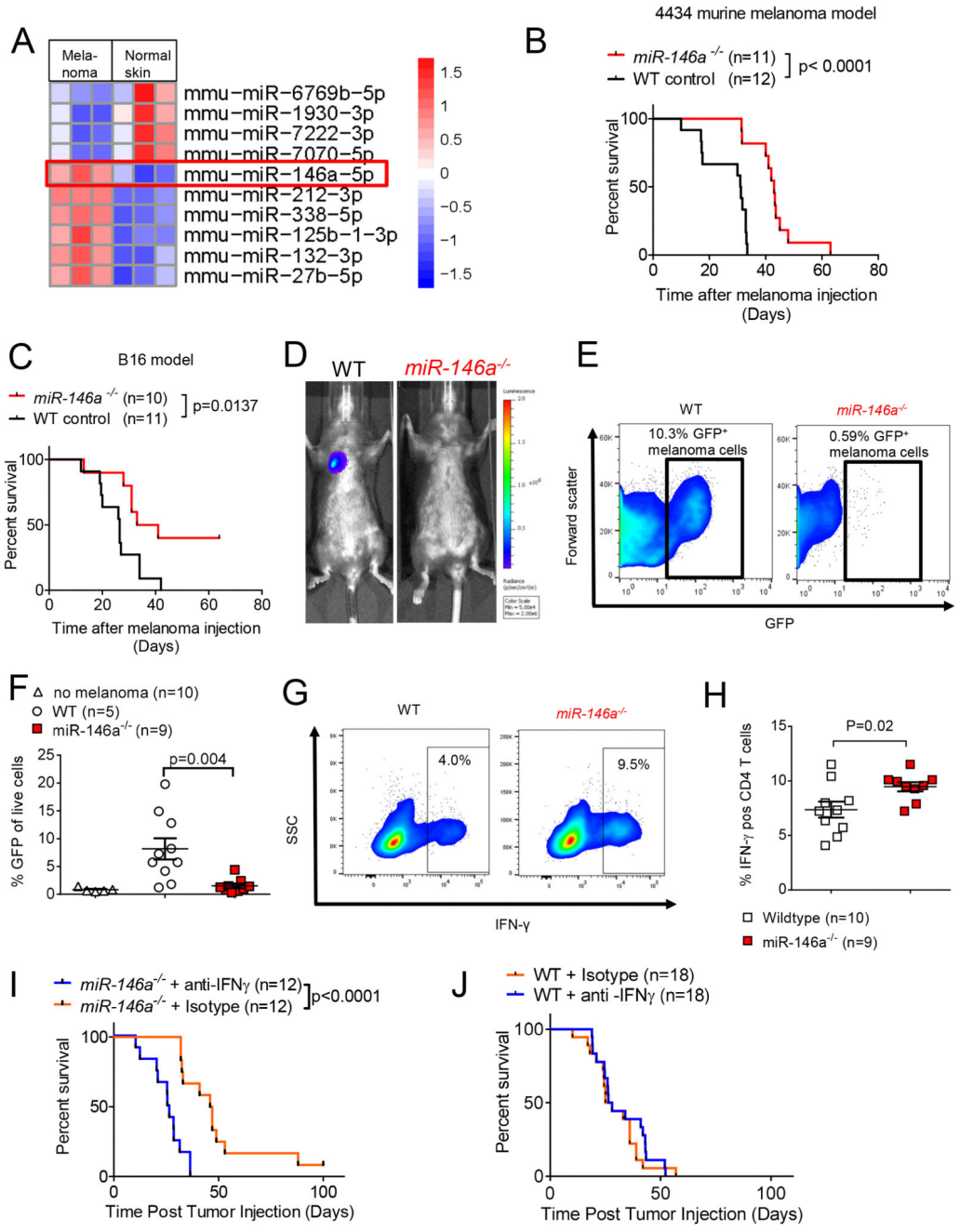


**Figure 1. *miR-146a*$^{-/-}$ mice experience reduced melanoma growth and survive better**

A. Relative expression, as microarray heatmap ("Z-score intensity"), of microRNAs isolated from primary melanoma and healthy skin of the 4-Hydroxytamoxifen treated BRaf$^{CA/}$ Pten$^{loxp}$/Tyr::CreER$^{T2}$ mouse or identically treated sibling without Tyr::CreER$^{T2}$, respectively. Top 10 differentially regulated miRNAs (adj. pvalue < .05) are displayed.

B. Kaplan-Meier survival curve of WT (black) or *miR-146a*$^{-/-}$ (red) mice injected intravenously with 2x10$^{6}$ 4434 murine melanoma cells.

C. Kaplan-Meier survival curve of WT (black) or *miR-146a*$^{-/-}$ (red) mice injected intravenously with 1x10$^4$ B16 Luc$^+$ murine melanoma cells.

D. Representative bioluminescence images (BLI) of mice described in (C) taken 21 days after tumor injection. For the bioluminescence imaging measurements the following parameters were kept constant for the WT and the *miR-146a*$^{-/-}$ group: amount of luciferin injected, type luciferin, exposure time and distance to camera.

E, F. Lungs from mice in (C) were isolated and digested on day 20-24 after tumor injection of the B16 melanoma model. Lung cell suspensions were analyzed for GFP$^+$ B16 melanoma cell composition.

E. Representative flow cytometry plots for GFP$^+$ B16 melanoma cells detected in the lungs of *miR-146a*$^{-/-}$ or WT control mice.

F. Quantification of GFP$^+$ B16 melanoma cells detected in the lungs of *miR-146a*$^{-/-}$ or WT control mice.

G. Representative FACS density plot of intracellular IFN-γ in CD4$^+$ T cells isolated from tumor free mice, day 22 after serial intraperitoneal injection with LPS. Cells were isolated from lymph nodes and spleens via MACS.

H. Scatter plot representing the percentage of intracellular IFN-γ positive cells of all CD4$^+$ T cells isolated from tumor-free mice, day 22 after LPS injection. Cells were isolated from lymph nodes and spleens via magnetic bead separation.

I. Survival of B16 melanoma bearing *miR-146a*$^{-/-}$ mice treated with anti-IFN-γ neutralizing antibody (blue) or isotype control (orange), (200μg/mouse/treatment).

J. Survival of B16 melanoma bearing wild type mice treated with anti-IFN-γ neutralizing antibody (blue) or isotype control (orange).



Europe PMC Funders Author Manuscripts

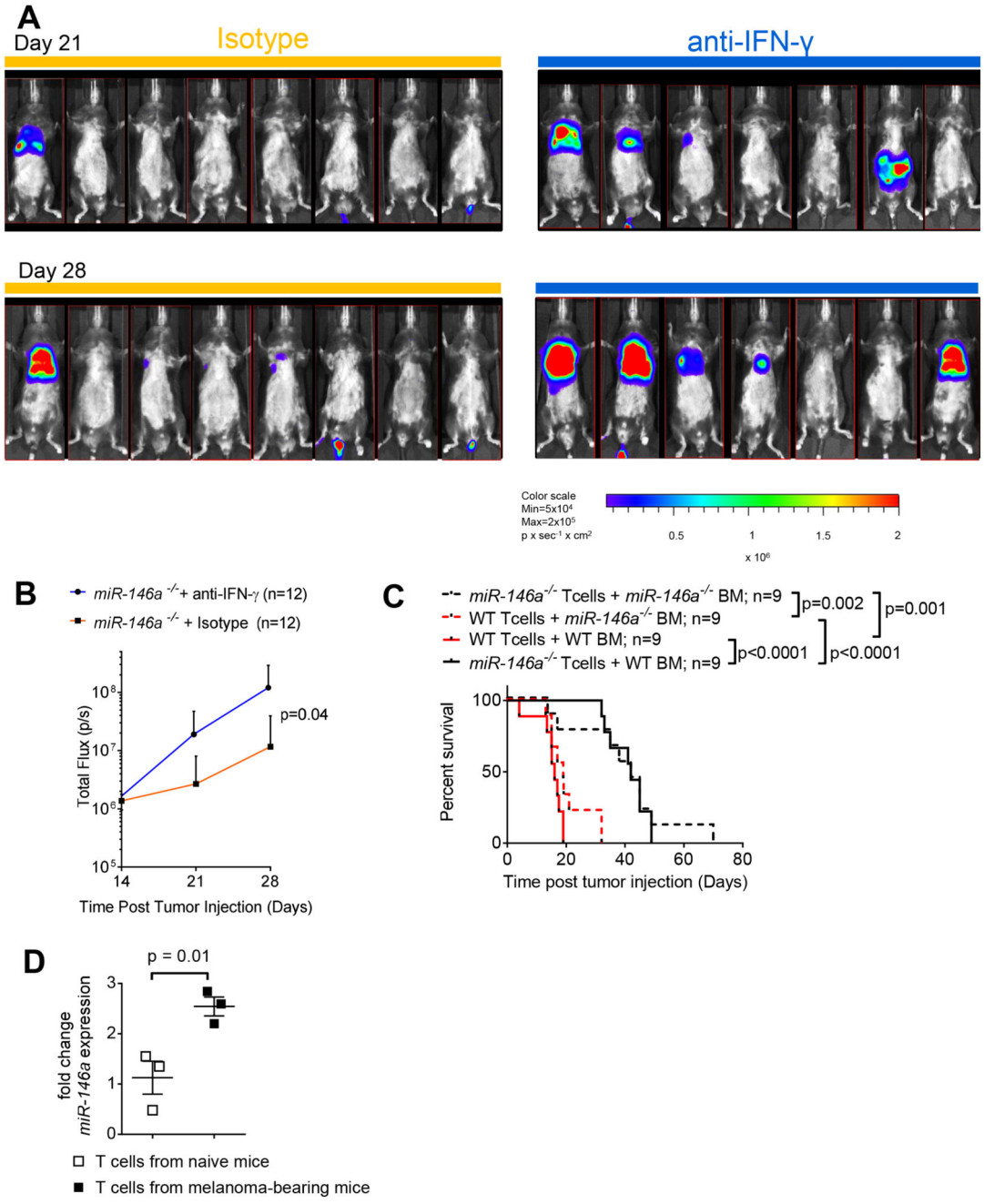


**Figure 2. Mechanistic relationship of miR-146a and IFN-γ in the melanoma microenvironment**

A. Representative BLI images taken on day 21 and day 28 after intravenous luc$^{+}$ B16 melanoma injection in *miR146a*$^{-/-}$ mice treated with IFN-γ neutralizing antibody (blue) or isotype control (orange). For the bioluminescence imaging measurements the following parameters were kept constant for the two groups: amount of luciferin injected, type luciferin, exposure time and distance to camera.

B. Graph of the means of proton flux (p/s/mouse) from the BLI measurements of experimental groups from (A).

C. Survival of B16 melanoma bearing mice that lacked miR-146a in different tissues. To generate hematopoietic-chimera, mice received 2x6Gy TBI, followed by intravenous BMT with wild type BM (solid lines) or *miR-146*$^{-/-}$ BM (dashed lines) on day -14. On day 0, CD4$^{+}$CD8$^{+}$ T lymphocytes isolated from the SLO of wild type (red lines) or *miR-146a*$^{-/-}$ (black lines) donors were transplanted intravenously. In addition on day 0, a total of 1x10$^{4}$ B16 melanoma cells was given intravenously per mouse.

D. T cells from the lungs of untreated mice or B16 melanoma bearing mice were isolated on day 24 after tumor injection by MACS sorting for CD4/8. RNA was isolated from the resulting T cells and analyzed by qPCR for miR-146a expression.



Europe PMC Funders Author Manuscripts

Europe PMC Funders Author Manuscripts

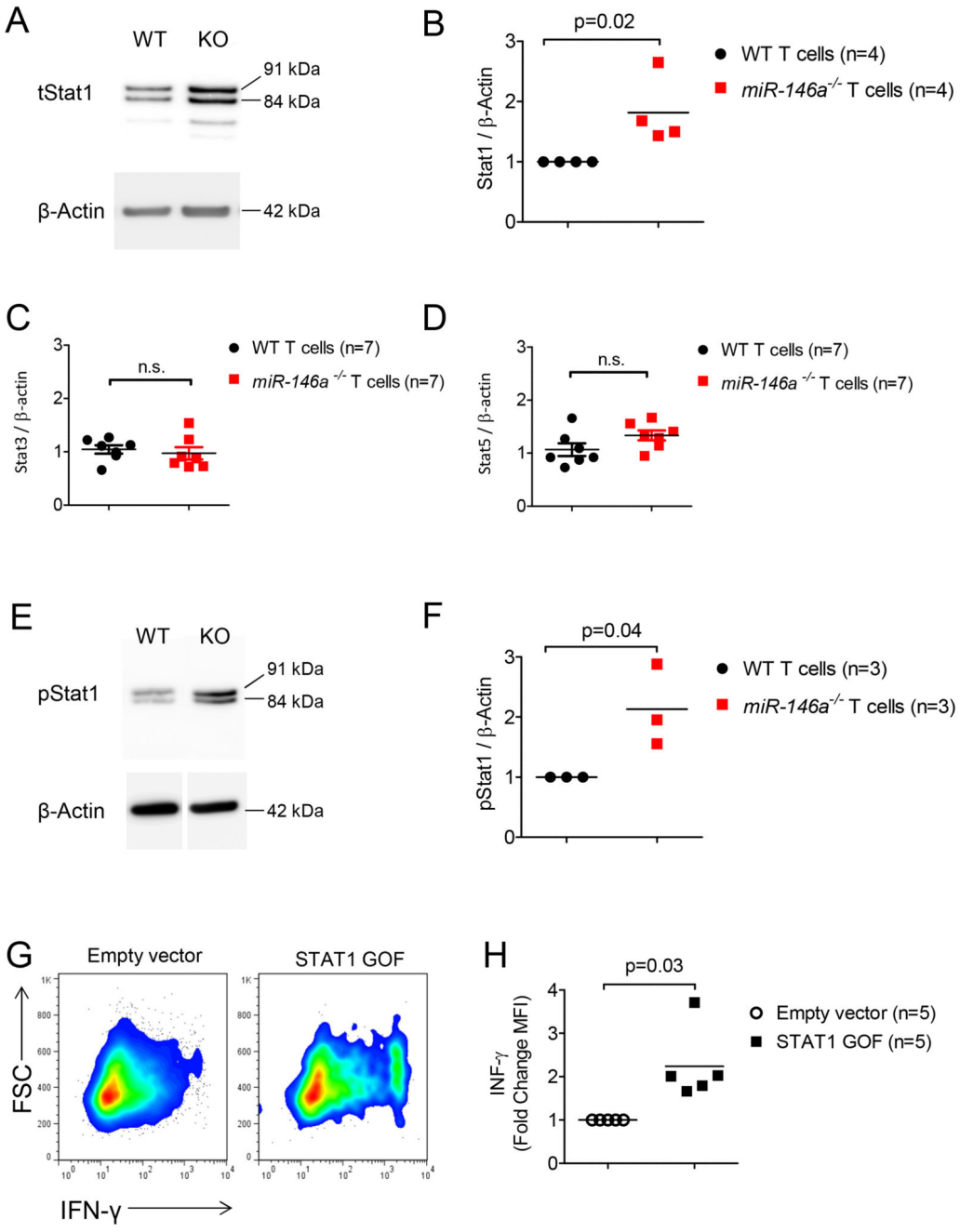


**Figure 3. *miR-146a*$^{-/-}$ T cells express higher STAT1 levels**

A. Representative western blot of STAT1 protein levels in CD4$^{+}$ and CD8$^{+}$ T cells isolated from the secondary lymphoid organs (SLO) of wild type and *miR-146a*$^{-/-}$ mice on day 21-24 after intravenous melanoma injection.

B. Scatter plot depicting the amount of STAT1 relative to β-actin control, performed as described in (A). Each data point represents an individual western blot result (biological replicate).

C. STAT3 protein levels in $CD4^+$ and $CD8^+$ T cells isolated from the secondary lymphoid organs (SLO) of wild type and *miR-146a*$^{-/-}$ mice on day 21-24 after intravenous melanoma injection. (Uncut western blot are shown in supplementary figure S5).

D. STAT5 protein levels in $CD4^+$ and $CD8^+$ T cells isolated from the secondary lymphoid organs (SLO) of wild type and *miR-146a*$^{-/-}$ mice on day 21-24 after intravenous melanoma injection. (Uncut western blot are shown in supplementary figure S5).

E. Representative western blot of phosphoSTAT1 protein levels in $CD4^+$, $CD8^+$ T cells isolated from the SLO of wild type and *miR-146a*$^{-/-}$ mice on day 21-24 after intravenous melanoma injection.

F. The scatter plot show the amount of phospho-STAT1 relative to β-actin control, performed as described in (A). Each data point represents an individual western blot result (biological replicate).

G. Representative flow cytometry density plot of intracellular IFN-γ in wildtype $CD4^+CD8^+$ primary T cells transfected with an empty vector or Stat-1 gain-of-function (GOF) vector.

H. Pooled Intracellular IFN-γ flow cytometry data of wildtype $CD4^+CD8^+$ primary T cells transfected with constitutively active STAT1 GOF or empty control vector.



Europe PMC Funders Author Manuscripts

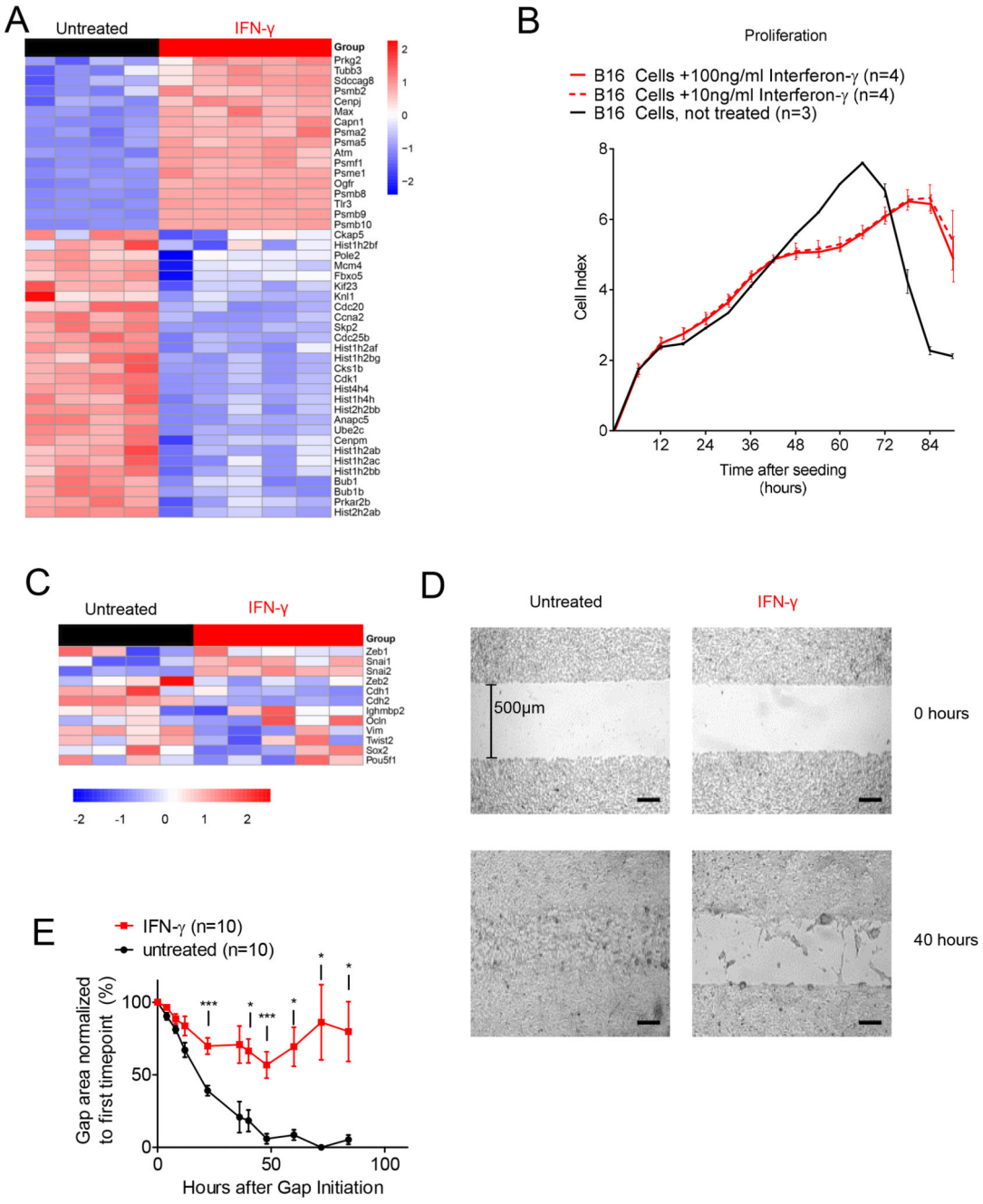


**Figure 4. IFN-γ inhibits melanoma proliferation and migration *in vitro*.**

A. mRNA expression of cell cycle associated genes of B16 melanoma cells. Heatmap ("Z-score intensity") generated based on microarray data from B16 melanoma cells incubated for 40 hours in media with or without 100ng/ml IFN-γ, as indicated.

B. Proliferation of B16 cells in serum-free media supplemented with IFN-γ (0ng/ml, 10ng/ml, or 100ng/ml). Cells were monitored for 90 hours and measurements were performed with an xCELLigence® assay.

C. mRNA expression (“Z-score intensity”) of EMT associated genes in B16 melanoma cells. Cells were treated with IFN-γ at a concentration of 100ng/ml for 40 hours prior to RNA isolation.

D. Migration of B16 melanoma cells in the presence or absence of IFN-γ (100ng/ml). The single time point images of scratch assay represent the situation at 0 hours and 40 hours. Initial gaps were 500μm. Scale bars are 200μm. All images were taken at 4x magnification.

E. The graph represents the gap area normalized to the time point = 0 hours. Gap closure was quantified using Mitobo plugin for ImageJ.



Europe PMC Funders Author Manuscripts

Europe PMC Funders Author Manuscripts

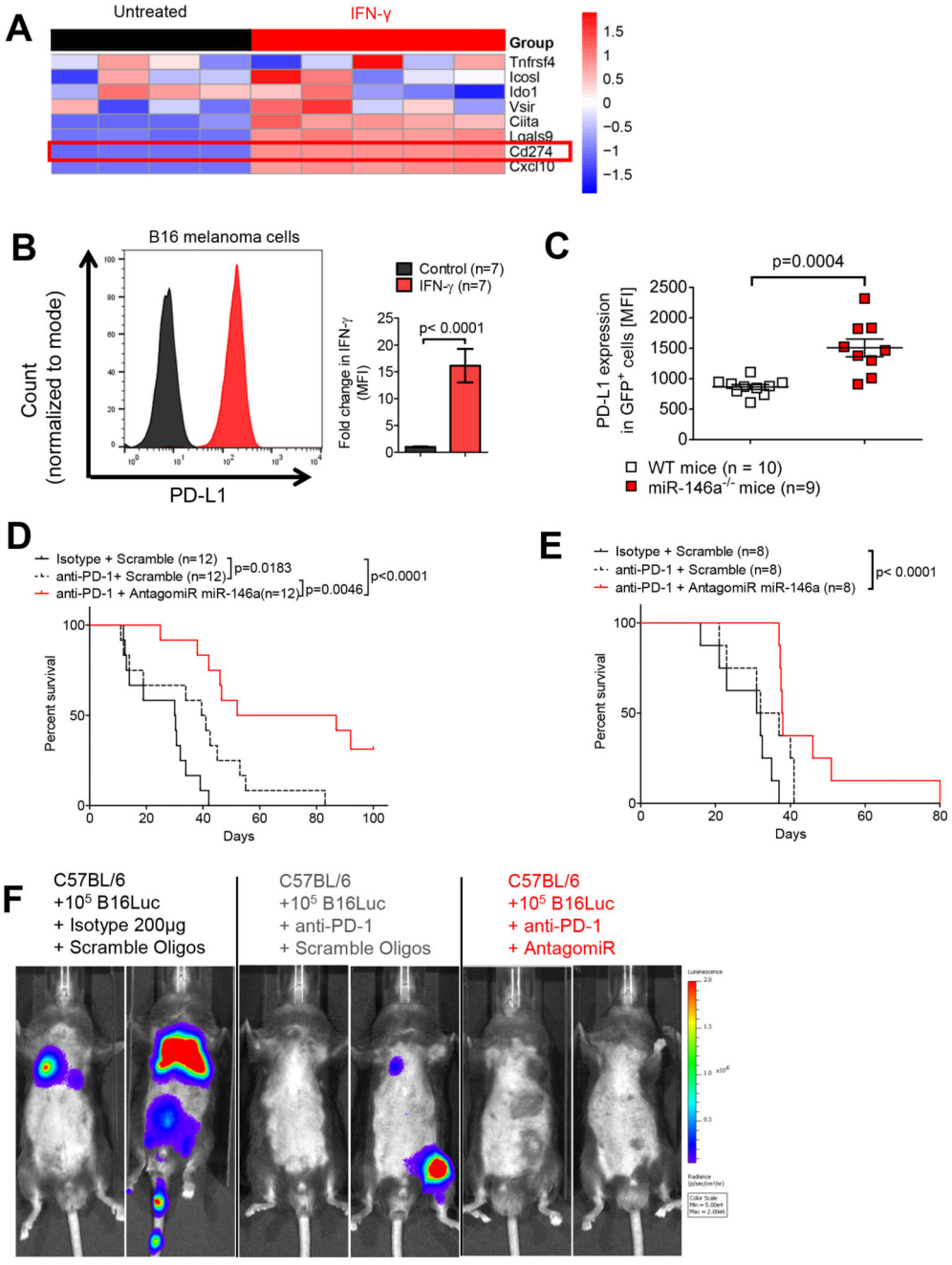


**Figure 5. IFN-γ increases PD-L1 levels on melanoma cells**

A. The heatmap displays the expression of genes related to cancer immunology ("Z-score intensity"). B16 melanoma cells were treated with IFN-γ at a concentration of 100ng/ml for 40 hours.

B. Representative flow cytometry histograms and cumulative data for PD-L1 levels are shown. The B16 melanoma cell line was exposed to IFN-γ (100ng/ml) for 24 hours before analysis. The treated cells appear in red and untreated controls appear in dark grey.

C. Lungs from mice in (Figure 1C) were isolated and digested on day 20-24 after tumor injection of the B16 melanoma model from WT or miR-146a KO mice. Lung cell suspensions were analyzed for PD-L1 levels on $GFP^+$ B16 melanoma cells via flow cytometry.

D. Survival of wild type C57BL/6 mice injected with $1x10^4$ B16 $Luc^+$ melanoma cells i.v. on day 0. Mice were treated days 1, 4, 8, 16, and 22 with anti-PD-1 antibody or Isotype IgG and on days 5 and 9 with anti-miR146a antagomiR or scramble antagomiR as indicated.

E. Survival curve of wildtype C57BL/6 mice injected with $2x10^6$ 4434 melanoma cells i.v on day 0. Mice were treated on days 1, 4, 8, 16 and 22 with anti-PD-1 antibody or Isotype IgG and on days 5 and 9 with anti-miR146a antagomiR or scramble antagomiR, as indicated.

F. Representative BLI images acquired on day 28 of mice from the experiment described in (D).



Europe PMC Funders Author Manuscripts

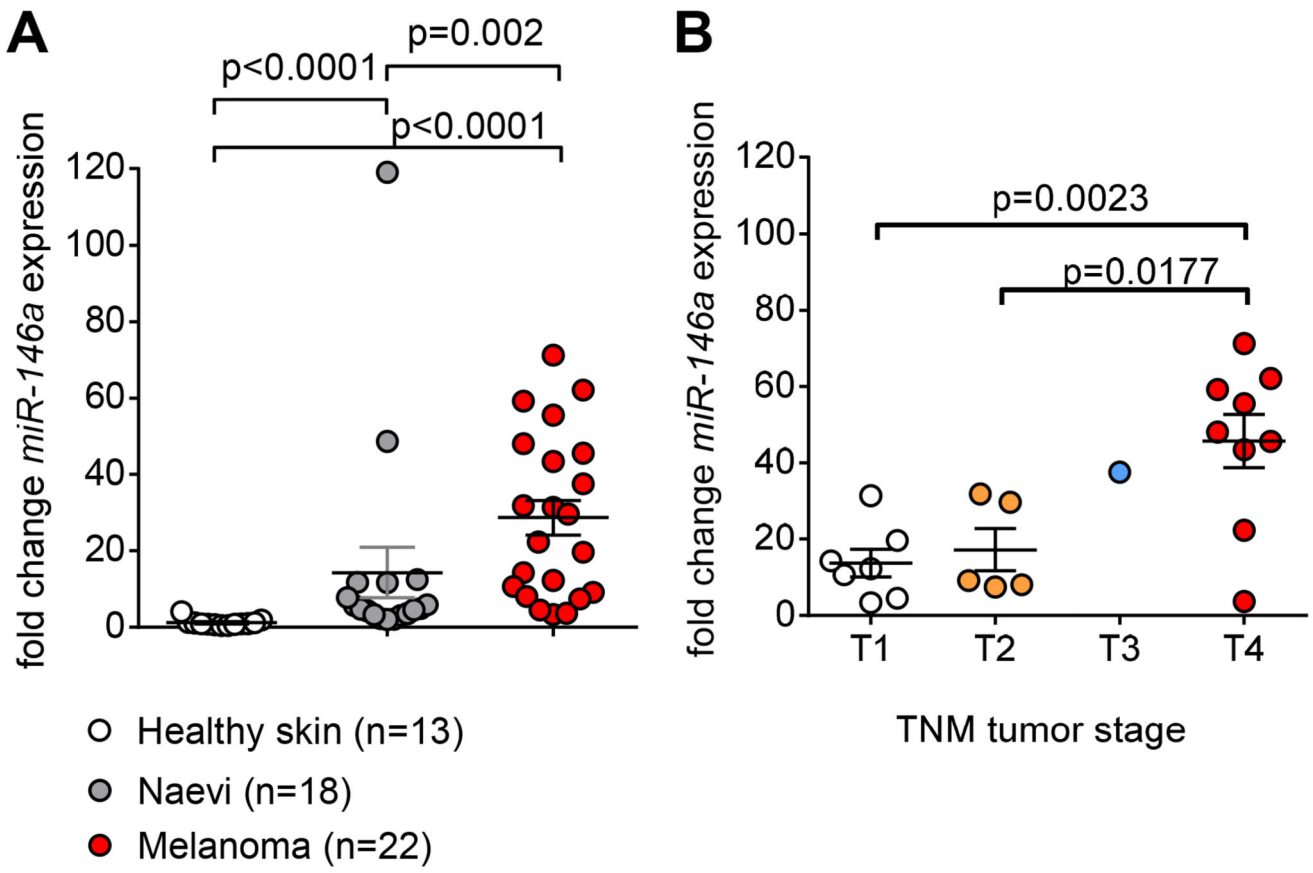


**Figure 6. miR-146a expression in human melanoma samples**

A. Comparative qPCR data displaying the miR-146a fold change relative to control snoRNA202 expression in human FFPE healthy skin, nevi, and melanoma.

B. Relative miR-146a fold change in human FFPE melanoma samples, correlated to TNM tumor size score.





Europe PMC Funders Author Manuscripts